THE JOURNAL OF BIOLOGICAL CHEMISTRY VOL. 289, NO. 32, pp. 22306–22318, August 8, 2014

Methylation Silencing of ULK2, an Autophagy Gene, Is Essential for Astrocyte Transformation and Tumor Growth*[S]

Received for publication, March 19, 2014, and in revised form, June 5, 2014 Published, JBC Papers in Press, June 12, 2014, DOI 10.1074/jbc.M114.567032

Sudhanshu Shukla[‡1], Irene Rosita Pia Patric[‡], Vikas Patil[‡], Shivayogi D. Shwetha[§], Alangar S. Hegde[¶], Bangalore A. Chandramouli[‖], Arimappamagan Arivazhagan[‖], Vani Santosh[§], and Kumaravel Somasundaram[‡2]

From the [‡]Department of Microbiology and Cell Biology, Indian Institute of Science, Bangalore 560012, India, the [¶]Sri Satya Sai Institute of Higher Medical Sciences, Bangalore 560066, India, and the Departments of [‖]Neurosurgery and [§]Neuropathology, National Institute of Mental Health and Neuro Sciences, Bangalore 560029, India

Background: Autophagy, a catabolic degradation process, has been shown to promote and inhibit cell growth.
Results: ULK2, an upstream autophagy initiator, is silenced by methylation in glioblastoma, and its ectopic expression inhibited astrocyte transformation and glioma cell growth through autophagy.
Conclusion: ULK2 down-regulation is important for the astrocyte transformation and tumor growth.
Significance: Autophagy inhibition is essential for glioma development.

Glioblastoma (GBM) is the most aggressive type of brain tumor and shows very poor prognosis. Here, using genome-wide methylation analysis, we show that G-CIMP+ and G-CIMP- subtypes enrich distinct classes of biological processes. One of the hypermethylated genes in GBM, ULK2, an upstream autophagy inducer, was found to be down-regulated in GBM. Promoter hypermethylation of ULK2 was confirmed by bisulfite sequencing. GBM and glioma cell lines had low levels of ULK2 transcripts, which could be reversed upon methylation inhibitor treatment. ULK2 promoter methylation and transcript levels showed significant negative correlation. Ectopic overexpression of ULK2-induced autophagy, which further enhanced upon nutrient starvation or temozolomide chemotherapy. ULK2 also inhibited the growth of glioma cells, which required autophagy induction as kinase mutant of ULK2 failed to induce autophagy and inhibit growth. Furthermore, ULK2 induced autophagy and inhibited growth in Ras-transformed immortalized Baby Mouse Kidney (iBMK) ATG5$^{+/+}$ but not in autophagy-deficient ATG5$^{-/-}$ cells. Growth inhibition due to ULK2 induced high levels of autophagy under starvation or chemotherapy utilized apoptotic cell death but not at low levels of autophagy. Growth inhibition by ULK2 also appears to involve catalase degradation and reactive oxygen species generation. ULK2 overexpression inhibited anchorage independent growth, inhibited astrocyte transformation *in vitro* and tumor growth *in vivo*. Of all autophagy genes, we found ULK2 and its homologue ULK1 were only down-regulated in all grades of glioma. Thus these results altogether suggest that inhibition of autophagy by ULK1/2 down-regulation is essential for glioma development.

Glioblastoma (GBM)[3] is the second most common type of primary brain tumor in adults (1). Despite significant advancements in therapy, which includes surgery, radiotherapy, and chemotherapy, the prognosis of GBM remains very poor (2). Genetic studies of glioma have identified many biomarkers (prognostic as well diagnostic) and therapeutic targets (3–5). In the recent past, studies on epigenetics, mainly on DNA methylation, have helped in the identification of many prognostic markers for GBM, which include MGMT promoter methylation and Glioma-CpG Island Methylator Phenotype (G-CIMP) (2, 6).

The promoter hypermethylation of tumor suppressor genes is a common mechanism of gene inactivation (7). Many known tumor suppressors including RB and p53 pathway genes are silenced in different cancers because of promoter hypermethylation (8). These tumor suppressor genes can be re-expressed using different methylase inhibitors, which can help in cancer chemotherapy (9). Indeed, use of 5-aza-2′-deoxycytidine has been approved for the treatment of myelogenous leukemia (10).

Autophagy, an evolutionarily conserved response to stress and starvation, is responsible for the degradation of non-functional organelles and proteins (11). Autophagy is also linked to cell death and is known as type II programmed cell death mechanism (12). Autophagic cell death process is quite different and more complex than that of type I programmed cell death or apoptosis. The exact mechanism of autophagic cell death is not known and is an interesting topic of investigation. Autophagy has been shown to promote or inhibit tumorigenesis based on the tumor type and stage (13, 14). The role of autophagy in gliomagenesis is not well understood. Reports have shown that the higher expression levels of the pivotal autophagy genes, LC3 and Beclin1 correlate with the better survival of GBM patients (15), suggesting the growth inhibitory effect of autophagy in GBM. Temozolomide, the drug of choice for GBM treatment,

* This study was supported by a grant from DBT, Government of India.
[S] This article contains supplemental Figs. 1–3 and Tables 1–5.
[1] Supported by a CSIR and IISc fellowship.
[2] A J. C. Bose Fellow of the Department of Science and Technology. To whom correspondence should be addressed: Department of Microbiology and Cell Biology, Indian Institute of Science, Bangalore 560012. Tel.: 91-80-23607171; Fax: 91-80-23602697; E-mail: skumar@mcbl.iisc.ernet.in.

[3] The abbreviations used are: GBM, glioblastoma; ULK1, Unc-like kinase 1; ULK2, Unc-like kinase 2; ATG, autophagy-related gene; G-CIMP, glioma-CpG island methylator phenotype; ROS, reactive oxygen species; DCFDA, 2′,7′-dichlorodihydrofluorescein diacetate; NHA, normal human astrocytes; NAC, *N*-acetyl cysteine; iBMK, immortalized baby mouse kidney.

utilizes autophagy mediated mechanism to induce cell death in glioma-derived cell lines (16). Further, rapamycin, an mTOR inhibitor, inhibits glioma cell lines *in vitro* and tumor growth in mouse xenograft model by inducing autophagy (17). While these reports suggest the growth inhibitory role for autophagy in glioma, autophagy inhibitors like Lys01 induces cell death in glioma cell lines (18). Similarly, hypoxia-induced autophagy was found to be cytoprotective leading to glioma cell survival (19). Thus autophagy appears to have a dual role in the chemosensitivity of glioma cells. However, there are no studies that have investigated the role of autophagy in glioma development.

In this study, we have performed genome-wide DNA methylation and identified ULK2, the autophagy inducer gene, as one of the hypermethylated and down-regulated genes in GBM compared with normal brain. We also demonstrate that ULK2 overexpression inhibited the glioma cell growth in an autophagy-dependent manner. Further, ULK2 inhibited the astrocyte transformation *in vitro* and tumor growth *in vivo*. Finally, we also provide evidence that the down-regulation of ULK1 (homologue of ULK2) and ULK2 is essential during gliomagenesis.

EXPERIMENTAL PROCEDURES

Patient Samples and Clinical Data—Tumor samples used for study were obtained from patients who were operated on at Sri Sathya Sai Institute of Higher Medical Sciences (SSSIHMS) and National Institute of Mental Health and Neurosciences (NIMHANS), Bangalore, India. Non-tumor brain tissue samples (anterior temporal lobe) obtained during surgery for intractable epilepsy were used as control samples. Tissues were bisected, and one-half was snap-frozen in liquid nitrogen and stored at −80 °C until DNA/RNA isolation. The other half was fixed in 10% neutral buffered formalin and processed for paraffin sections. These sections were used for the histopathological grading of tumor and immunohistochemical staining. The written consent from all patients was obtained prior to initiation of the study as per IEC guidelines and approval.

A total of 108 GBM samples and 16 normal brain samples were used in this study. Out of these samples, 64 GBMs and 9 normal brain samples were used for real time RT-PCR validation of the ULK2 gene, and 44 GBM and 8 normal brain samples were used for the Infinium methylation assay.

Genomic DNA Extraction and Sodium Bisulfite Conversion—DNA from these tissues was isolated using QIAamp DNA mini kit (Qiagen). DNA was quantified and used for bisulfite conversion with the EZ DNA methylation kit (Zymo Research) as suggested by the manufacturer. In brief, 1 μg of DNA was mixed with 5 μl of M-dilution buffer, and the final volume was made up to 45 μl and incubated at 42 °C for 20 min. After incubation, 100 μl of CT Conversion Reagent was mixed and incubated in a thermocycler overnight (95 °C 30 s, 50 °C 1 h, 16 cycles). Bisulfite-converted DNA was then column-purified using a Zymo-Spin IC column and eluted in water. This bisulfite converted DNA was then used for the Infinium methylation assay as suggested by the manufacturer.

Differential Methylation and Other Statistical Analysis—We utilized Infinium methylation27 BeadChip (Illumina, San Diego, CA) for DNA methylation analysis. Infinium array interrogates 27,578 CpG sites covering 14,495 genes. DNA methylation analysis was performed using 44 GBM and 8 normal samples as described before (20). Briefly, intensities obtained from the Infinium array was used to calculate the beta value, the methylation index, using the following formula: β value = (signal intensity of M Probe)/[(signal intensity of M + U probes) +100].

We performed a two-sided *t* test, and *p* values were adjusted using the method of Benjamini and Hochberg, to select the probes that are significantly differentially methylated in GBM compared with normal. It identified 567 CpGs hypermethylated and 1097 CpGs hypomethylated in GBM compared with normal; thus making the total differentially methylated CpGs in GBMs to 1664. Further, to select the probes with biologically meaningful methylation differences, we removed all the CpGs, which were showing the average beta value difference less than 0.3 between GBMs and normal, which identified 261 CpGs as hypermethylated and 427 CpGs as hypomethylated. Then the list of differentially methylated genes was compared with the expression data generated by The Caner Genome Atlas (TCGA), to find out the genes whose expression level negatively correlate with methylation. On comparison, we found that the genes corresponding to 62 CpGs out of 261 hypermethylated CpGs to be down-regulated, and the genes corresponding to 55 CpGs out of 428 hypomethylated CpGs to be up-regulated in GBM. This correlation further reduced the functionally relevant differentially methylated CpGs to 117 (62 hypermethylated and 55 hypomethylated).

All quantitative data were recorded as median ± S.D. A comparison between two groups was performed by the two-sided *t* test using GraphPad Prism 5.01. To compare the transcript levels of ULK1, ULK2, ULK3, ULK4, ATG101, FIP200, BECN1, UVRAG, Bif1, ATG12, ATG13, ATG4C, ATG5, and ATG7 in normal brain and GBMs, the expression values were obtained from The Cancer Genome Atlas (TCGA) dataset (Agilent and Affymetrix), GSE22867 dataset, and REMBRANDT (3) dataset. A two-sided *t* test was performed to obtain the significance in the difference.

G-CIMP Identification—We utilized the method described by Noushmehr *et al.* (6) to identify the G-CIMP population in our dataset. Briefly, we took the methylation value of 1503 probes for all the patients of our lab dataset and performed K-means clustering using R software. The program divided the patients into 3 groups. The smallest cluster consisting of 5 patients was considered as G-CIMP positive as they showed increased methylation of majority of 1503 probes and also increased overall survival, though survival difference was not significant due to a lower number of G-CIMP+ samples (supplemental Fig. SF1*A*, *B*, and *C*).

Cell Lines and Plasmids—Glioma cell lines U138, U343, LN229, U251, U87, and U373 were grown in DMEM while SVG cells were grown in MEM medium. The medium was supplemented with 10% FBS, penicillin, and streptomycin. Normal human astrocytes were a kind gift from Dr. Abhijit Guha. Wild-type iBMK and ATG5$^{-/-}$ iBMK cells were a kind gift from Prof. Eileen White, Cancer Institute of NJ (20) and were grown in DMEM with 10% FBS, penicillin, and streptomycin.

ULK2 overexpression construct (Myc and DDK tagged) and vector control was obtained from Origene. Mouse ULK2, mutant mouse ULK2, human ULK2, human ULK1, mouse ULK1 overexpression constructs were obtained from Addgene. mCherry-tagged LC3 was a kind gift from Dr. Tamotsu Yoshimori, Osaka University, Japan.

Bisulfite Sequencing—CpG island of ULK2 promoter and bisulfite sequencing primers were identified using MethPrimer. The PCR mixture contained 100 nM of each primer, 200 ng of bisulfite-treated DNA, 1.25 units of TaqDNA Polymerase (NEB), 0.2 μM deoxynucleotide triphosphate (dNTP; each), and 4 mM $MgSO_4$ in a final volume of 20 μl. PCR products were purified and cloned in pGEM-T easy vector system (Promega), which was then used to transform into the DH5a bacteria. The transformed colonies were then grown in LB medium with ampicillin. The plasmid was isolated using QIAprepSpin-Miniprep Kit (Qiagen) and sequenced using M13 primers. Sequences were analyzed using the web-based tool QUMA.

RNA Isolation and Real-time Quantitative RT-PCR Analysis—RNA was isolated using TRI reagent (Sigma), and cDNA was made using the high capacity cDNA reverse transcription kit (Life Technologies). For real-time PCR ABI PRISM 7900 HT Sequence Detection System (Life Technologies) was used. Expression was analyzed using GAPDH, 18 S RNA, and RPL35a as a reference gene and the ΔΔCt method (4).

5-Aza-2′-deoxycytidine Treatment—Cells (1.5×10^6 per 60-mm dish) were plated and incubated for 12 h. After 12 h, they were treated with different concentrations of 5-aza-2′-deoxycytidine for 72 h or 120 h. After treatment, total RNA was isolated and used for real-time PCR.

Immunohistochemistry (IHC)—IHC was performed for the protein expression of ULK-2 on 52 samples that included 8 control samples and 44 GBM tumors. Formalin-fixed paraffin-embedded sections of 4-μm thickness were collected on silane-coated slides and deparaffinized., Antigen retrieval was done by heat treatment in Tris EDTA buffer (pH 9). After the initial processing steps, sections were incubated overnight at 4 °C with anti-ULK-2 (from Sigma-Aldrich, (C-HPA009027: diluted to 1:25), followed by incubation with secondary antibody (QD440-XAK, Biogenex), and the reaction was visualized using 3,3′-diaminobenzidine (Sigma-Aldrich) as a chromogenic substrate. A positive control (normal human cerebellum) and a negative control slide (in which the primary antibody is omitted) were included with each batch of staining. A visual semi-quantitative grading scale was applied to assess the intensity of immunoreactivity. The assessment was scored as absent staining, moderate, and strong staining.

COBRA Analysis—Genomic DNA was isolated from the different cell lines using Qiagen DNA prep kit. gDNA was then used for bisulfite conversion using a Zymo bisulfite conversion kit. A part of CpG island of ULK2 promoter was amplified by PCR. The PCR mixture contained 100 nM of each primer, 500 ng of bisulfite-treated DNA, 2.5 units TaqDNA Polymerase (NEB), 0.2 μM deoxynucleotide triphosphate (dNTP; each), and 4 mM $MgSO_4$ in a final volume of 50 μl. The PCR product was then gel purified using Fermentas gel purification column and digested with BstUI (NEB). Digested PCR products were separated on 2.2% agarose gels and visualized. BstU1 recognizes CGCG and cleaves the DNA. Bisulfite treatment converts unmethylated C to U (eventually in T during PCR amplification). Based on the methylation status of DNA, BstU1 cleaves (methylated DNA) or fails to cleave (unmethylated DNA).

Colony Formation Assay—Colony suppression assays were done in 6-well plates. Cells (0.4×10^6 per well) were plated and transfected with different expression construct using Lipofectamine 2000 transfection reagent. The cells were selected in G418 supplemented medium at 24 h after transfection. Resistant cells were maintained for 3–4 weeks in culture. After incubation, colonies were fixed and stained with crystal violet and counted.

Stable Cell Line Generation—For stable generation, cells were (0.4×10^6 per well) plated and transfected with different plasmids using Lipofectamine 2000 transfection reagent. After 24 h of transfection. The transfected cells were selected with G418 for 3 weeks and individual clones transferred to a new plate and grown. Some cells were simultaneously harvested to confirm increased expression of the transfected gene by real-time PCR. These cells were then used for different studies.

Proliferation Assay—For the proliferation assay, 5×10^4 cells were plated in 6-well plates and allowed to settle for 24 h. Cell proliferation was monitored using a ViCell counter (Backman Coulter) by counting the cell number every alternate day.

LC3 Confocal Microscopy—Cells were plated on coverslips in a 6-well plate. After 12 h of plating, cells were transfected with LC3-mCherry and ULK2 or vector and incubated for 8 h, before media was changed. After 36 h of transfection, cells were fixed with 4% paraformaldehyde and washed with PBS. Cells were then mounted on slide using antifade as mounting media. For LC3 confocal analysis of Ras-transformed iBMK $ATG5^{+/+}$ and $ATG5^{-/-}$ cells, cells were plated on coverslips in a 6-well plate and incubated for 12 h. These cells were then transfected with ULK2 or vector and incubated for 8 h, before media was changed. After 36 h of transfection, cells were fixed with 4% paraformaldehyde and washed with PBS. Cells were then mounted on slides using antifade as mounting media.

In Vitro Transformation Assay—Immortalized human astrocytes (with E6/E7/hTERT) were plated in a 6-well plate (0.4×10^6 cells per well). Cells were then transfected with Ras either with vector or with the ULK2 overexpression construct using Lipofectamine 2000 transfection reagent. After 24 h of transfection, cells were plated in soft agar to select the transformed colonies.

In Vivo Tumor Formation—Animal experiments were performed according to the local animal ethics commission protocols. 100 μl of single cell suspension of 3×10^6 cells were injected subcutaneously. The tumor diameters were measured using calipers, and measurement was done every 3rd day. Tumor volumes were determined using the following formula: $V = D \times d2/2$ (V, tumor volume; D, the biggest dimension; d, the smallest dimension).

CNV Calculation—For copy number variation, UCSC cancer genome browser was used. Copy number variation was calculated using the TCGA dataset ($n = 576$). For each gene, CNV was calculated and shown in the form of a boxplot. The box represents the first and third quartiles, and the middle line rep-

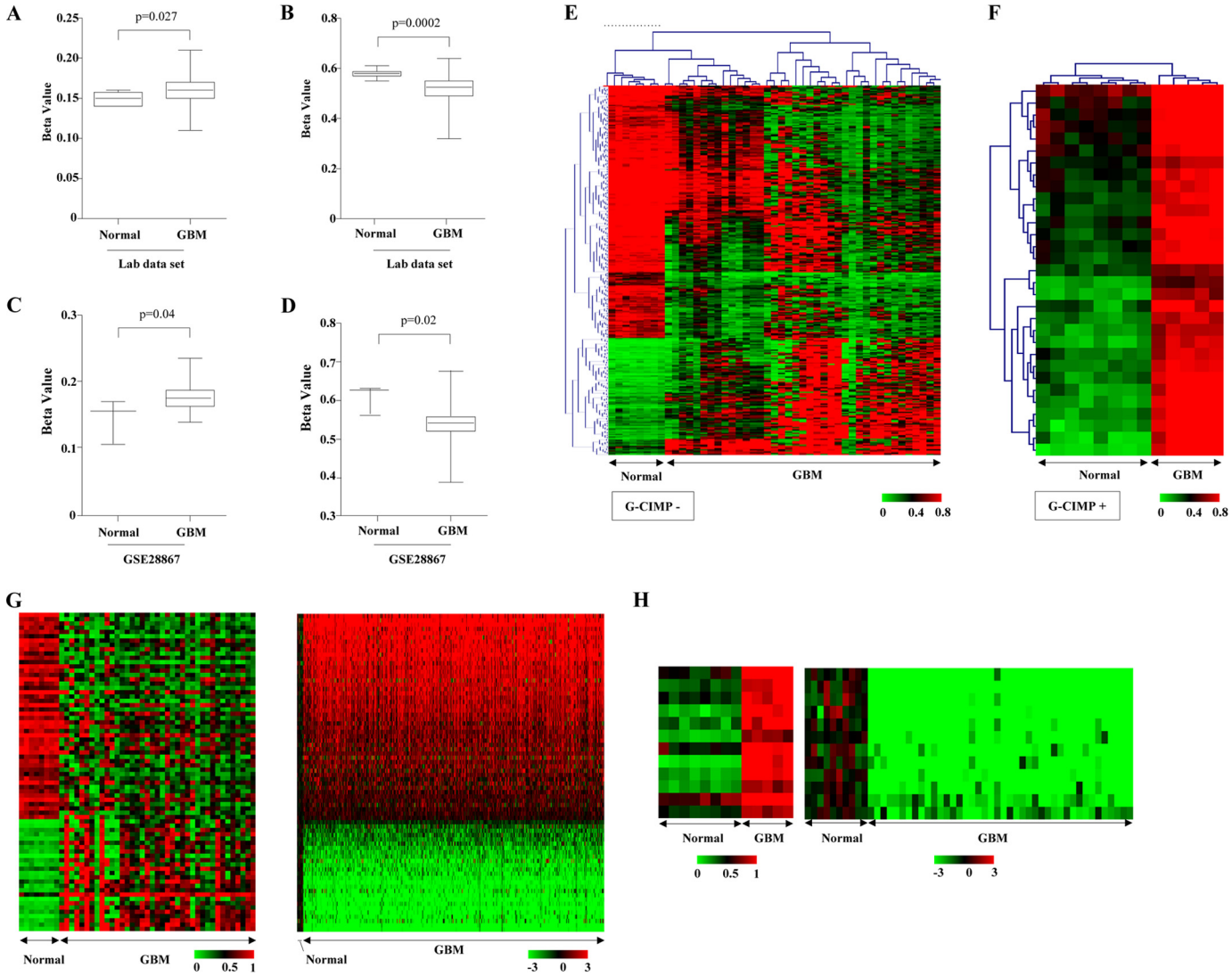

FIGURE 1. **Methylation analysis of normal brain and GBM samples.** *A*, beta values of CpGs located in the CpG Island were taken from the lab dataset. The average beta values of these CpGs was calculated in normal brain and GBM samples and plotted. *B*, beta values of CpGs located in non CpG Island area were taken from the lab dataset. The average beta values of these CpGs were calculated in normal brain and GBM samples and plotted. *C*, beta values of CpGs located in CpG Island were taken from the GSE28867 dataset. The average beta values of these CpGs was calculated in normal brain and GBM samples and plotted. *D*, beta values of CpGs located in non CpG Island area were taken from GSE28867 dataset. The average beta values of these CpGs were calculated in normal brain and GBM samples and plotted. *E*, heat map of beta values of significantly differentially methylated CpGs between G-CIMP- and normal brain samples. A dual color code was used of *red* for increased beta value and *green* for decreased beta value. *F*, heat map of beta values of significantly differentially methylated CpGs between G-CIMP+ and normal brain samples. A dual color code was used indicating *red* for increased beta value and *green* for decreased beta value. *G*, heat map showing significantly differentially methylated (*left*; our dataset) and expressed genes (*right*; expression values from the TCGA dataset) in G-CIMP, compared with normal. A dual color code was used indicating *red* for increased beta value and *green* for decreased beta value for methylation; and for expression, *red* indicates increased expression, and *green* indicates decreased expression. *H*, heat map showing significantly differentially methylated (*left*; our dataset) and expressed genes (*right*; expression values from TCGA dataset) in G-CIMP + compared with normal. A dual color code was used indicating *red* for increased beta value and *green* for decreased beta value for methylation, and for expression; *red* indicates increased expression, and *green* indicates decreased expression.

resents the median. The color intensity is proportional to the deviation from the median.

RESULTS

Genome-wide DNA Methylation Analysis of G-CIMP+ and G-CIMP- GBM Reveals Enrichment of Distinct Biological Processes—To dissect the DNA methylation pattern of GBM, we performed genome wide methylation analysis ($n = 44$ GBM and $n = 8$ normal brain samples) using Infinium methylation27 BeadChip array. Differential methylation analysis revealed hypermethylation of the CpGs in CpG islands in GBM compared with normal samples ($p = 0.027$), while the CpGs from non-CpG islands showed hypomethylation in GBM compared with normal ($p = 0.0002$) in our lab dataset (Fig. 1, *A* and *B*). This observation was also confirmed using another dataset-GSE28867 (Fig. 1, *C* and *D*). Thus, as observed in other cancers (21), GBM also shows hypomethylation of CpGs from non-CpG island areas and hypermethylation of CpGs from CpG islands.

Next, to find differentially methylated genes in GBM, we utilized a highly rigorous statistical analysis (see "Experimental Procedures" for detail) and identified 62 CpGs (54 genes) to be

hypermethylated and down-regulated and 55 CpGs (51 genes) to be hypomethylated and up-regulated in GBM (supplemental Table ST1). Glioma-CpG island methylator phenotype (G-CIMP) corresponds to a distinct subtype of GBM with concerted hypermethylation at a large number of loci (6). G-CIMP+ tumors have a unique methylation profile compared with G-CIMP-tumors and associated with IDH1 mutation (6).The analyses of the G-CIMP+ and G-CIMP- tumors independently, identified several group-specific (G-CIMP-: 284 genes; G-CIMP+: 31 genes) and common ($n = 6$ genes) differentially methylated genes compared with normal brain samples (Fig. 1, *E* and *F*; supplemental Table ST2). It is interesting to note that all the 6 genes (ULK2, RPL39L, HIST1H1A, RTKN, LEP, and APCDD1), which are differentially methylated in both groups, were found to be hypermethylated in GBM. Further analysis revealed that only a subset of these genes (G-CIMP-: 74, G-CIMP+: 17, and common: 3) were found to be showing opposite transcript regulation, suggesting they are the physiologically relevant differentially methylated genes (Fig. 1, *G* and *H*; supplemental Table ST3). Three genes that were found to be hypermethylated and down-regulated in GBM, are RPL39L, ULK2, and HIST1H1A. To understand the biological significance of G-CIMP+ and G-CIMP-specific differential methylome, gene ontology analysis was carried out. We found that different biological processes are enriched in these two groups (supplementary Table ST4). While the G-CIMP+ tumors, which are less aggressive with good prognosis are enriched for cell death pathways, catabolic processes, and protein kinase cascade, the G-CIMP- tumors, which are more aggressive with poor prognosis, are enriched for various development and differentiation pathways, inflammatory, and immune response pathways.

ULK2 Is Hypermethylated and Down-regulated in Glioma—ULK2, which is methylated and silenced as shown above, was particularly interesting as it is essential for autophagy induction. Further analysis revealed that ULK2 (CpG ID: cg12324629) is hypermethylated in our lab dataset and TCGA and GSE28867 datasets (Fig. 2*A*). The ULK2 transcript is down-regulated in GBM from four datasets and also in glioma-derived cell lines compared with control brain samples (Fig. 2, *B* and *C*). A significant negative correlation was seen between methylation and transcript levels of ULK2 (Fig. 2*D*). The ULK2 protein expression determined by IHC showed a moderate to strong staining among glial cells. While the majority of control brain samples showed positive staining (6/8; 75%), only 37.5% (11/44) of GBM samples were positively stained (Fig. 2*E*). Bisulfite sequencing validated the hypermethylation of the ULK2 promoter in GBM and glioma cell lines as against normal brain samples (Fig. 2*F*; supplemental Table ST5). The methylation inhibitor, 5-aza-2′-deoxycytidine, treatment resulted in the re-expression of ULK2 transcript, and protein (Fig. 2, *G* and *H*, respectively). 5-Aza-2′-deoxycytidine-treated cells showed reduced methylation of ULK2 promoter as analyzed by COBRA (Fig. 2*I*). We conclude from these experiments that ULK2 expression is silenced by promoter methylation in GBM.

ULK2-induced Autophagy Mediates Cell Growth Inhibition—Autophagy can promote both cell survival and cell death in a context-dependent manner (22). Since ULK2 is methylated and silenced in GBM, we hypothesized that ULK2-induced autophagy may be growth inhibitory in glioma. Ectopic expression of human ULK2 (hULK2) along with mCherry LC3 in LN229 glioma cells resulted in autophagy induction as seen by a severalfold increase in mCherryLC3 puncta formation (Fig. 3*A*) and increased (7.5-fold) accumulation of LC3-II (Fig. 3*B*, compare *lane 4* with *1*). In addition, autophagy induced by nutrient starvation or temozolomide treatment is further increased upon ectopic expression of hULK2 (Fig. 3*B*, compare *lane 5* with *2* and *6* with *3* and Fig. 3*C*). Ectopic expression of hULK2 also resulted in suppression of colony formation (Fig. 3*D*) and reduced proliferation (Fig. 3*E*) in glioma cell line (s). Re-expression of endogenous ULK2 by methylase inhibitor treatment resulted in autophagy induction in a ULK2-dependent manner as seen by the change in the accumulation of LC3 II (Fig. 2*H*; compare *lane 2* with *1* and *4* with *3*). In addition, methylase inhibitor treatment inhibited cell growth, which was significantly abrogated upon ULK2 silencing by siRNA (Fig. 2*J*).

Autophagy induction appears to be essential for ULK2-induced growth inhibition as a kinase mutant (K39T) of mouse ULK2 (mULK2 mutant), deficient for autophagy induction, failed to inhibit proliferation, while wild-type mouse ULK2 (mULK2), and wild-type hULK2 efficiently inhibited proliferation in LN229 cells (Fig. 3*F*).To further validate this observation, we used Ras-transformed iBMK ATG5$^{+/+}$ and ATG5$^{-/-}$ cells (23). Ectopic expression of mULK2-induced autophagy efficiently in iBMK ATG5$^{+/+}$ cells as seen by increased mCherry LC3 puncta formation and the appearance of the LC3 II band but not in iBMK ATG5$^{-/-}$ cells (Fig. 3, *G* and *H*, respectively). Both hULK2 and mULK2 suppressed colony formation and proliferation efficiently in iBMK ATG5$^{+/+}$ cells (Fig. 3, *I* and *J*, respectively). As expected, the kinase mutant of mULK2 failed to suppress colony formation and proliferation. However, in iBMK ATG5$^{-/-}$ cells, both ULK2 and mULK2 failed to inhibit colony formation and proliferation (Fig. 3, *I* I and *J*, respectively). All these results indicate that autophagy is essential for ULK2-mediated growth inhibition.

Role of Apoptosis and Reactive Oxygen Species (ROS) in ULK2-mediated Cell Death—High levels of autophagy have been shown to inhibit growth by apoptosis-dependent cell death mechanisms (24). To dissect the mechanism of growth inhibition by ULK2, apoptotic cell death by various methods and DNA synthesis by BrdU incorporation were measured. Ectopic overexpression of hULK2 alone induced apoptotic cell death minimally as seen by a slight increase in annexin V-positive cells (Fig. 4*A* compare *bar 2* with *1*), cleaved caspase level (Fig. 3*B*, compare *lane 4* with *1*), and caspase 3/7 activity (Fig. 4*B*). BrdU incorporation assay confirmed significant DNA synthesis inhibition in cells with ectopic ULK2 overexpression (Fig. 4*C*). Thus, the growth inhibition by ULK2 appears to involve both apoptosis and DNA synthesis inhibition. However, ectopic hULK2 overexpression in temozolomide pre-treated cells induced apoptosis significantly as seen by increased annexin V-positive cells (Fig. 4*A*, compare *bar 4* with *3*). This was further supported by an increase in cleaved caspase levels (Fig. 3*B*, compare *lane 6* with *3*) and increased caspase 3/7 activity (Fig. 4*B*). Similarly, starvation-induced apoptosis also increased upon hULK2 overexpression as seen by the increase

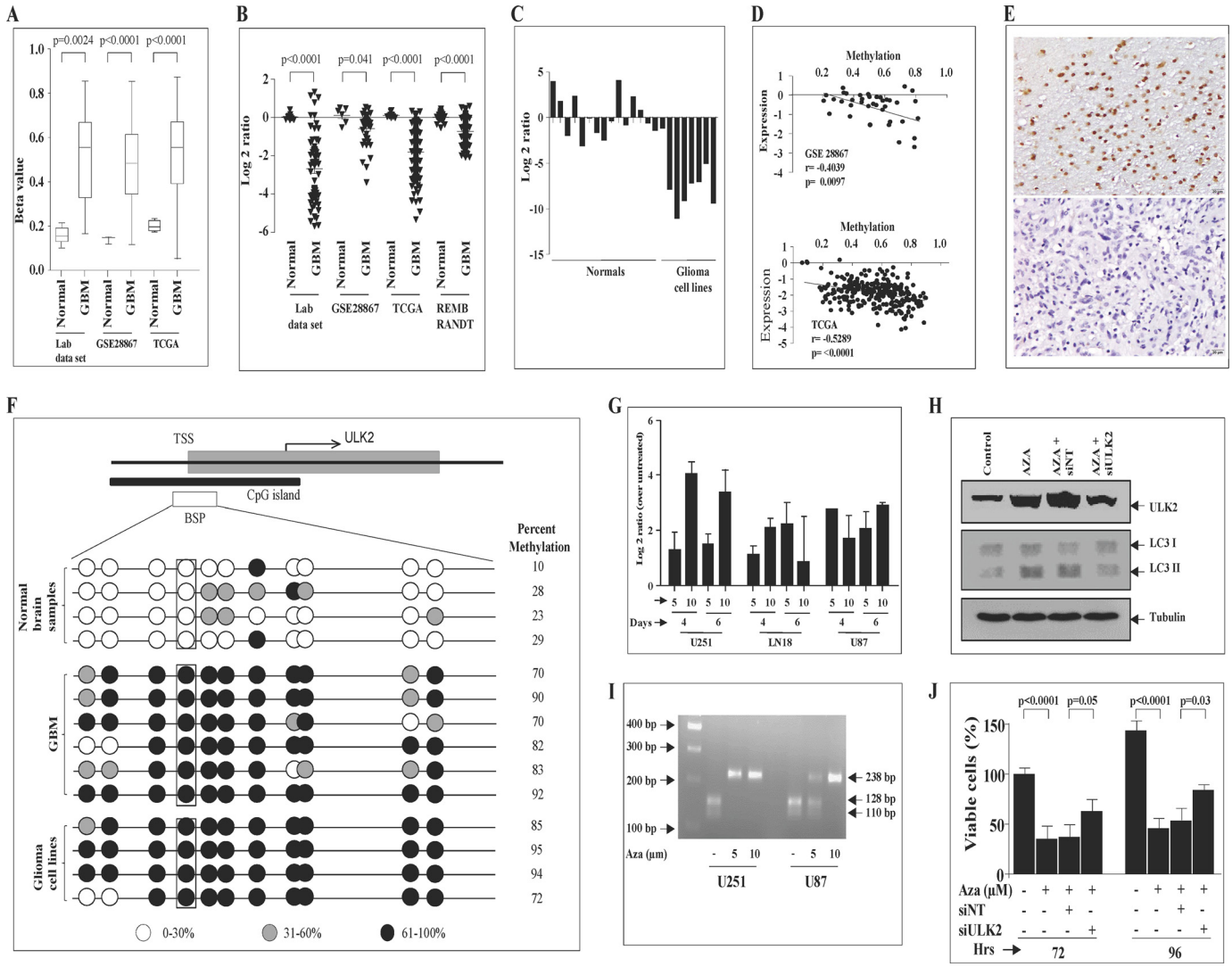

FIGURE 2. **ULK2 is methylation silenced in GBM.** *A*, beta values of ULK2 in normal brain (lab dataset $n = 8$, TCGA dataset $n = 4$, GSE28867 dataset $n = 3$) and GBM samples (lab dataset $n = 44$, TCGA dataset $n = 264$, GSE28867 dataset $n = 50$) were taken and plotted in a *box plot*. The *t* test was performed between normal brain and GBM samples, and the *p* values are indicated. *B*, ULK2 transcript levels derived from indicated datasets were plotted. The *t* test was performed between normal brain (our dataset $n = 8$, TCGA dataset $n = 4$, GSE28867 dataset $n = 3$, REMBRANDT $n = 28$) and GBM samples (our dataset $n = 44$, TCGA dataset $n = 264$, GSE28867 dataset $n = 50$, REMBRANDT $n = 227$), and the *p* values are indicated. *C*, ULK2 transcript measured in different normal brain samples, Immortalized Human Astrocytes (NHA) and glioma cell lines using qRT-PCR are plotted. The expression is normalized using the average of ULK2 expression in normal brain samples and shown. *D*, correlation graph showing significant negative correlation between methylation and expression of the ULK2 gene in GSE28867 and TCGA dataset. *E*, sections of normal and GBM FFPE samples were probed with ULK2 antibody. Representative images show positive staining in normal glial cells and negative staining in GBM cells. (Original magnification ×160). *F*, bisulfite sequence PCR analysis (BSP) of the ULK2 promoter. Each *row* represents the methylation pattern of one sample. The percentage methylation of promoter methylation was calculated and shown in supplemental Table ST4. The percentage methylation was calculated as total percentage of methylated cytosines from 7–10 randomly sequenced colonies. *TSS*, transcription start site. *Box* represents the CpG analyzed by Infinium array. *G*, total RNA was isolated from glioma cell lines after treatment with 5-aza-2-deoxy cytidine (*Aza*), and the ULK2 transcript level was quantified by RT-qPCR. For each sample, the fold change in gene expression was calculated over its mean expression in untreated samples. *H*, total protein was isolated from LN229 cells treated or untreated with 5-aza-2-deoxy cytidine (*Aza*) transfected with siNT or siULK2 and ULK2, LC3 I/II and tubulin protein levels were measured. *I*, U87 and U251 cells were treated with a given concentration of aza-2-deoxy cytidine (*Aza*) for 4 days, and genomic DNA was isolated. COBRA was performed to see the methylation status of part of the ULK2 promoter. *J*, LN229 cells treated or untreated with 5-aza-2-deoxy cytidine (*Aza*) transfected with siNT or siULK2 and plated. Viable cells visualized by Trypan Blue staining were measured at different time points and plotted.

in cleaved caspase levels (Fig. 3*B*, compare *5* with *2*). Thus, these results suggest ULK2-mediated growth inhibition indeed involves apoptosis-dependent cell death mechanisms. To further investigate the role of apoptosis in ULK2-mediated growth inhibition, ULK2-induced cell death was monitored under conditions where either autophagy or apoptosis was inhibited. While the autophagy inhibitor (3-methyladenine) treatment inhibited ULK2-induced cell death very efficiently, the apoptosis inhibitor (Z-VAD-FMK) treatment inhibited ULK2-mediated cell death very minimally (Fig. 4, *D* and *E*). However, in temozolomide-treated cells, ULK2-induced cell death was inhibited very efficiently by both autophagy and apoptosis inhibitors (Fig. 4, *D* and *E*). These results suggest that apoptosis appears to play an important role in ULK2-induced cell death in particular when there is induction of high levels of autophagy.

Autophagy-mediated cell death also involves selective degradation of catalase with the resultant increase in cellular reactive oxygen species (ROS) level (25). We found that ectopic overexpression of mULK2, but not the kinase mutant, induced autophagy as seen by LC3 II formation and degradation of cat-

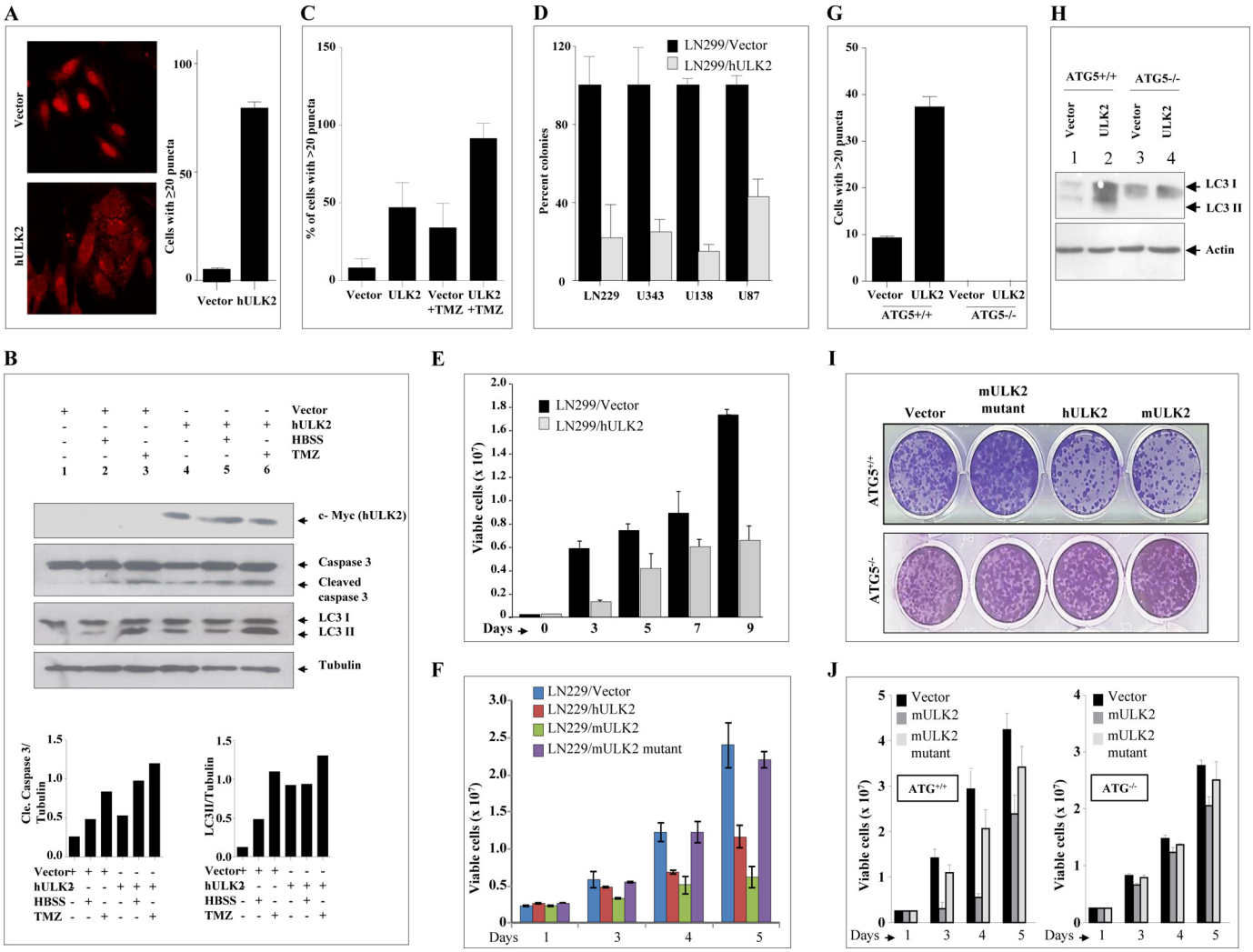

FIGURE 3. **Wild-type ULK2 increases autophagy and inhibits GBM cell growth.** *A*, LN229 cells were co-transfected with mCherry-tagged LC3 protein and vector or hULK2 plasmid. mCherry LC3 puncta were visualized using confocal microscopy. Number of cells with >20 puncta were counted and plotted. *B*, LN229/Vector and LN229/hULK2 cells were grown in DMEM with serum (*lanes 1* and *4*; for 12 h), DMEM with serum and Temozolomide (*lanes 3* and *6*; for 12 h), and Hanks buffered salt solution (*lanes 2* and *4*; for 4 h), and the total protein was isolated. The expression of indicated proteins was analyzed by Western blot. *Bar diagrams* shows quantification of cleaved caspase 3 and LC3II bands normalized with tubulin. *C*, LN229 cells were co-transfected with m-cherry-tagged LC3 protein and vector or ULK2 plasmid and treated with temozolomide or control. LC3 m-cherry puncta were visualized using confocal microscopy. Number of cells with >20 puncta were counted and plotted. *D*, indicated cell lines were transfected with vector or hULK2 and G418-resistant colonies were selected. The colonies were counted, and mean colony counts are displayed as percentage of vector control. *E*, LN229/Vector or LN229/ULK2 stable cells were plated, and the viable cells, by Trypan Blue staining, were measured at different time points and plotted. *F*, LN229/Vector or hULK2 or mULK2 or mutant mULK2stable cells were plated, and viable cells, by Trypan Blue staining, were counted and plotted. *G*, ATG5$^{+/+}$ and ATG5$^{-/-}$ iBMK cells transfected with vector control and ULK2 and checked for the LC3 puncta formation using confocal microscopy. Number of cells with >20 puncta were counted and plotted below. *H*, total protein from ATG5$^{+/+}$ and ATG5$^{-/-}$ iBMK stable with vector or ULK2 was isolated, and levels of LC3 I and II were measured using Western blot. The LC3 II band intensity normalized to acting control is shown. *I*, ATG5$^{+/+}$ and ATG5$^{-/-}$ iBMK/cells were transfected with vector or mutant mouse ULK2 (mULK2 mutant) or human ULK2 (hULK2) or mouse ULK2 (mULK2), and G418-resistant colonies were selected. Colonies were stained with crystal violet and photographed. *J*, ATG5$^{+/+}$ iBMK/Vector or mULK2 or mutant mULK2 stable and ATG5$^{-/-}$ iBMK Vector or mULK2 or mutant mULK2 cells were plated, and viable cells (Trypan Blue staining) were counted and plotted.

alase as seen by reduced catalase (Fig. 4*F*, compare *lanes 3* and *2* with *1*). ULK2-overexpressing cells also had significantly increased cellular ROS levels compared with vector-transfected LN229 cells (Fig. 4*G*, compare *bar 2* with *1*) and was effectively abrogated by pre-treatment of cells with ROS scavenger (*N*-acetyl cysteine; NAC) (Fig. 4*G* compare *bars 4* with *2*). Further, LN229 cells with increased ROS upon ULK2 overexpression showed increased cell death and were rescued by NAC treatment (Fig. 4*H*, compare *bars 3* and *4* with *1* and *2*). Next to confirm the importance of autophagy in ULK2-mediated ROS generation and cell death, we used Ras-transformed iBMK ATG5$^{+/+}$ and ATG$^{-/-}$ cells. In ATG$^{+/+}$ cells, mULK2 overexpression induced ROS and cell death, which was rescued by the addition of NAC (Fig. 4, *I* and *J*, respectively). However, in ATG$^{-/-}$ cells, mULK2 failed to induce ROS and cell death (Fig. 4, *K* and *L*, respectively). These results conclude that ROS generation plays an important role in ULK2-mediated cell death.

ULK2 Overexpression Inhibits in Vitro Astrocyte Transformation and in Vivo Tumor Growth—Autophagy is a known inhibitor of the initial transformation event (26). Since ULK2-induced autophagy inhibits cell growth, we hypothesized that ULK2 overexpression should inhibit transformation. Ectopic expression of hULK2 in LN229 inhibited anchorage-independent growth as seen by a significant reduction in colony forma-

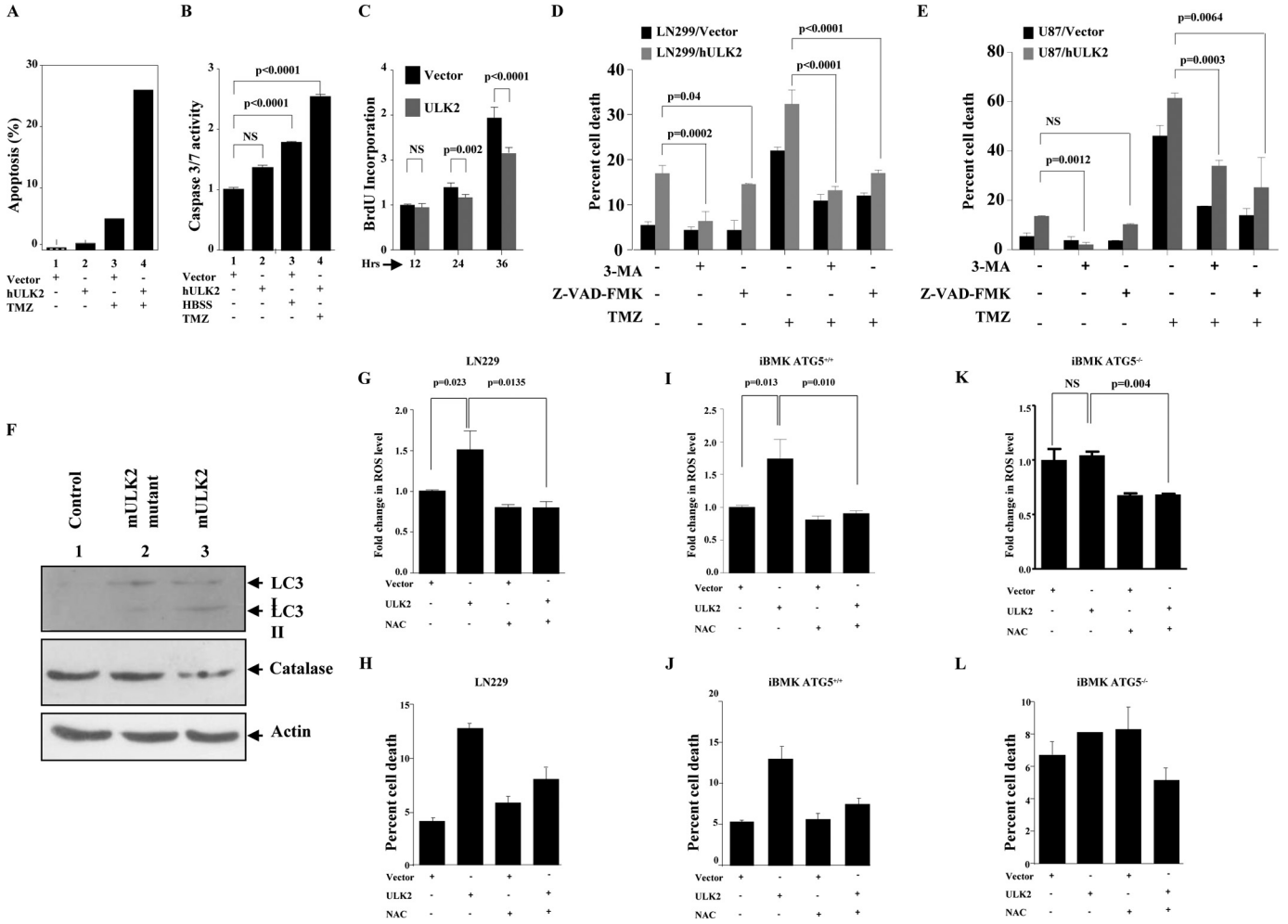

FIGURE 4. **Role of apoptosis and ROS in ULK2-mediated cell death.** *A*, LN229/Vector and LN229/hULK2stable cells were treated with vehicle (DMSO), ortemozolomide (TMZ; 250 μM), and apoptosis was checked using PI-Annexin V double staining. The percentage of Annexin V-positive cells is shown. *B*, LN229/Vector and LN229/hULK2 stable cells were treated with vehicle (DMSO) or temozolomide (TMZ; 250 μM), and caspase3/7 activity was checked. The change in caspase3/7 activity compared with control is shown. *C*, LN229/Vector and LN229/hULK2 stable cells were treated with BrdU for a given time point, and BrdU incorporation was measured using the BrdU ELISA kit. The change in BrdU incorporation compared with vector control cells is shown. *D*, LN229/Vector and LN229/hULK2 stable cells were treated as indicated, and the percentage of dead cells (Trypan Blue staining) compared with total cells was calculated and plotted. *E*, U87/Vector and U87/hULK2 stable cells were treated as indicated, and the percentage of dead cells (Trypan Blue staining) compared with total cells was calculated and plotted. *F*, total protein extract from LN229/Vector or mULK2 or mutant mULK2stable cells was isolated, and the expression level of indicated proteins was checked using Western blot. *G*, ROS level in LN229/Vector or mULK2 untreated or treated with NAC (5 mM) was measured using DCFDA assay. The mean intensity of ROS was plotted and shown. *H*, cell death in LN229/Vector or mULK2 untreated or treated with NAC was measured using Trypan Blue staining and plotted as percentage cell death and shown. *I*, ROS level in ATG5$^{+/+}$stable with Vector or mULK2 untreated or treated with NAC (5 mM) was measured using the DCFDA assay. The mean intensity of ROS was plotted and shown. *J*, cell death in ATG5$^{+/+}$stable with Vector or mULK2 untreated or treated with NAC was measured using Trypan Blue staining and plotted as percentage cell death and shown. *K*, ROS level in ATG5$^{-/-}$ stable with Vector or mULK2 untreated or treated with NAC (5 mM) was measured using the DCFDA assay. The mean intensity of ROS was plotted and shown. *L*, cell death in ATG5$^{-/-}$ stable with Vector or mULK2 untreated or treated with NAC was measured using Trypan Blue staining and plotted as percentage cell death and shown.

tion soft agar (Fig. 5*A*, compare *bar 2* with *1*). We also tested the effect of ectopic introduction of hULK2 on the ability of Ras to transform immortalized (E6/E7 and hTERT) astrocytes. We found that Ras-induced transformation was inhibited significantly by hULK2 (Fig. 5*B*, compare *bar 2* with *1*). Further to confirm these observations *in vivo*, we tested the ability of mULK2 to inhibit the Ras-transformed iBMK ATG$^{+/+}$ and ATG$^{-/-}$ cells to form tumors in nude mice. While the iBMK ATG$^{+/+}$ vector stable cells formed tumors efficiently, the iBMK ATG$^{+/+}$ mULK2 stable cells failed to form tumors (Fig. 5*C*, compare *orange line* with *blue line*). In contrast, iBMK ATG$^{-/-}$ cells formed small tumors, as observed by others (23). However, there was no significant difference in tumor formation capacity of vector or mULK2 stable cells (Fig. 5*D*, compare *orange line* with *blue line*). These observations confirm that ULK2 inhibits astrocyte transformation *in vitro* and tumor growth by inducing autophagy.

ULK1 and ULK2, but Not Other Autophagy Genes, Are Inactivated by Down-regulation in GBM—Essential autophagy genes, ATG5, ATG7, and BECN1 are known to be down-regulated in some cancers (14, 27). To explore the importance of autophagy genes besides ULK2, in the regulation of autophagy during transformation, we analyzed the transcript profiles of all autophagy pathway genes in TCGA and REMBRANDT expression datasets. This analysis showed that ULK1, ULK2, and FIP200 are the only down-regulated genes in GBM, while the

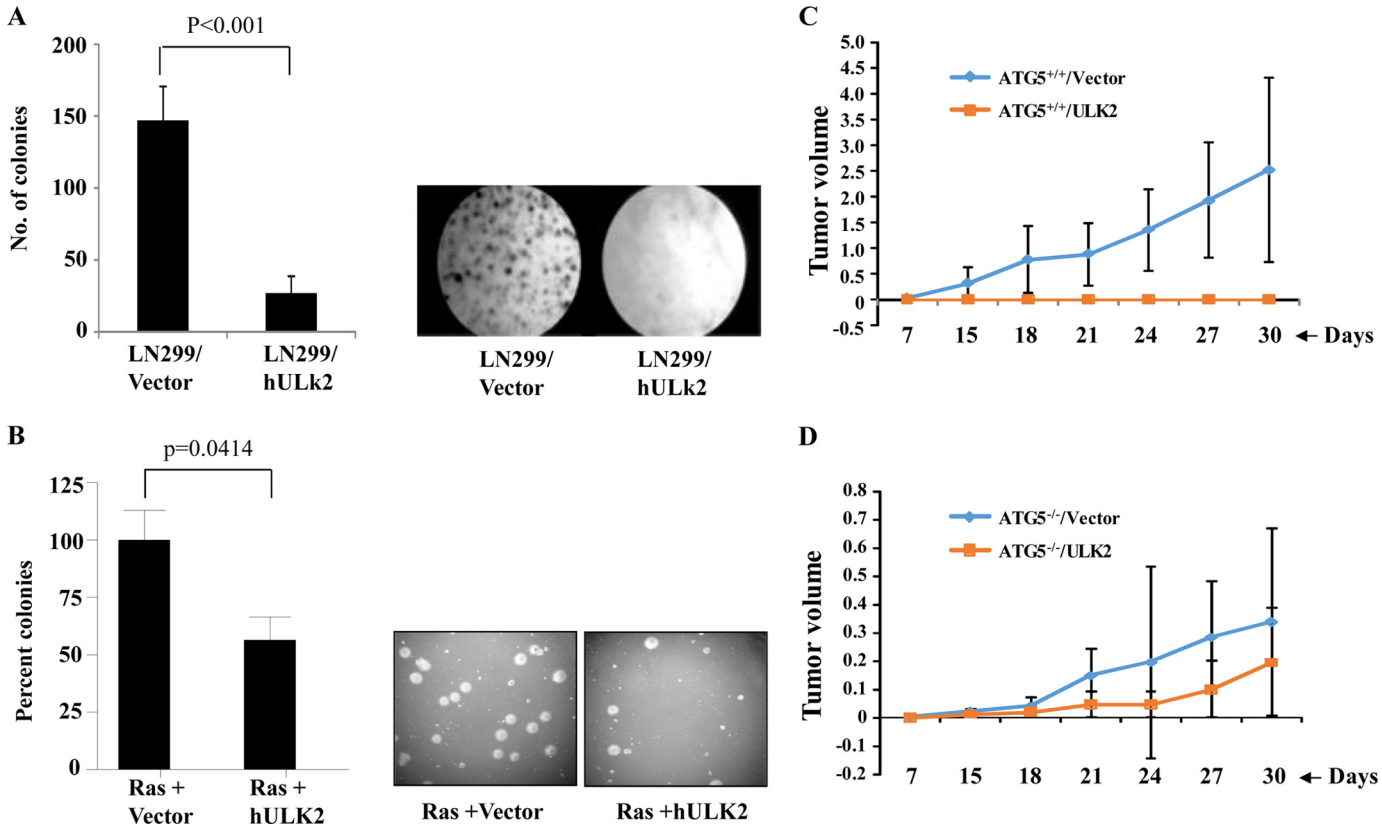

FIGURE 5. **ULK2 inhibits *in vitro* transformation and *in vivo* tumor growth.** *A*, LN229/Vector and LN229/hULK2 stable cells were subjected to soft agar colony formation, and the number of colonies was counted and plotted. Representative pictures are shown on the *right side*. *B*, immortalized NHA were co-transfected with vector + Ras V12 or with hULK2 + Ras V12. After 24 h of transfection, cells were plated in soft agar and transformed colonies were selected and shown. NHA by themselves did not form colonies in soft agar. Number of colonies formed were counted and plotted. *C*, Ras-transformed iBMK ATG5$^{+/+}$ stable cells with vector or mULK2 (3×10^6 cells) were injected into the right flank of nude mice (NIH nu/nu; 10 animals each), and the tumor volume was measured at indicated days. *D*, Ras-transformed iBMK ATG5$^{-/-}$ stable cells with vector or mULK2 (3×10^6 cells) were injected into the right flank of nude mice (NIH nu/nu; 10 animals each), and the tumor volume was measured at the indicated days. The difference in tumor size between the two groups was found to be nonsignificant.

remaining genes are not consistently differentially regulated between GBM and normal brain samples (supplemental Fig. SF2). We also found both ULK1 and ULK2 transcripts are down-regulated in both diffuse astrocytoma (grade II) and anaplastic astrocytoma (grade III), which again confirms the down-regulation of these two genes essential for astrocyte transformation (Fig. 6*A*). Further, we found that ULK1 is not differentially methylated in GBM compared with normal brain samples, unlike ULK2, which suggests the mechanism of down-regulation of ULK1 may be different (Figs. 6*B* and 2*A*). However, copy number variation is not the underlying cause for ULK1 and ULK2 down-regulation (supplemental Fig. SF3). We also found that ULK1, similar to ULK2, is also able to inhibit colony formation in glioma cells (Fig. 6*D*). This observation confirms that ULK1 is also down-regulated in GBM and has a redundant function similar to ULK2.

We explored the mechanism of ULK1 down-regulation in GBM. As ULK1 is a known target of p53 (28), and the p53 pathway is inactivated in the majority of GBM, we checked the effect of p53 on ULK1 transcript and protein levels. Adriamycin-induced p53 activation increased ULK1 transcript and protein levels in p53 wild-type cells (U87 and A172), which lead to autophagy induction but not in p53 mutant cells (LN229), suggesting that p53 is a transcriptional activator of ULK1 (Fig. 6, *E* and *F*). Thus we conclude that down-regulation of both ULK1 and ULK2 is important in inhibiting autophagy, which is essential for astrocyte transformation.

DISCUSSION

Genetic and epigenetic alterations are primary and important events for the development of cancers. Among epigenetic alterations, changes in DNA methylation of cytosine residues in CpG dinucleotide play a pivotal role in not only initial transformation but also on other aspects of cancer-like migration and invasion. While the majority of the cancer genome, which includes non CpG islands of repetitive DNA sequence genome, is subjected to undermethylation, hypermethylation is seen in CpG islands present at the promoters of many genes (29, 30). Further, CpG Island Methylator Phenotype (CIMP) identifies a distinct molecular subtype in a number of cancers including glioblastoma (6, 31, 32). In glioblastoma, G-CIMP tumors appear to be enriched with pro neural subtype tumors and IDH1 mutations (6). Recently, IDH1 mutation has been found to be the cause of CIMP development in gliomas (33). Thus, the differences in DNA methylation within GBM have been addressed extensively. In contrast to these studies, while there have been few studies on differential methylation in GBM in comparison to normal brain samples, the role of DNA methy-

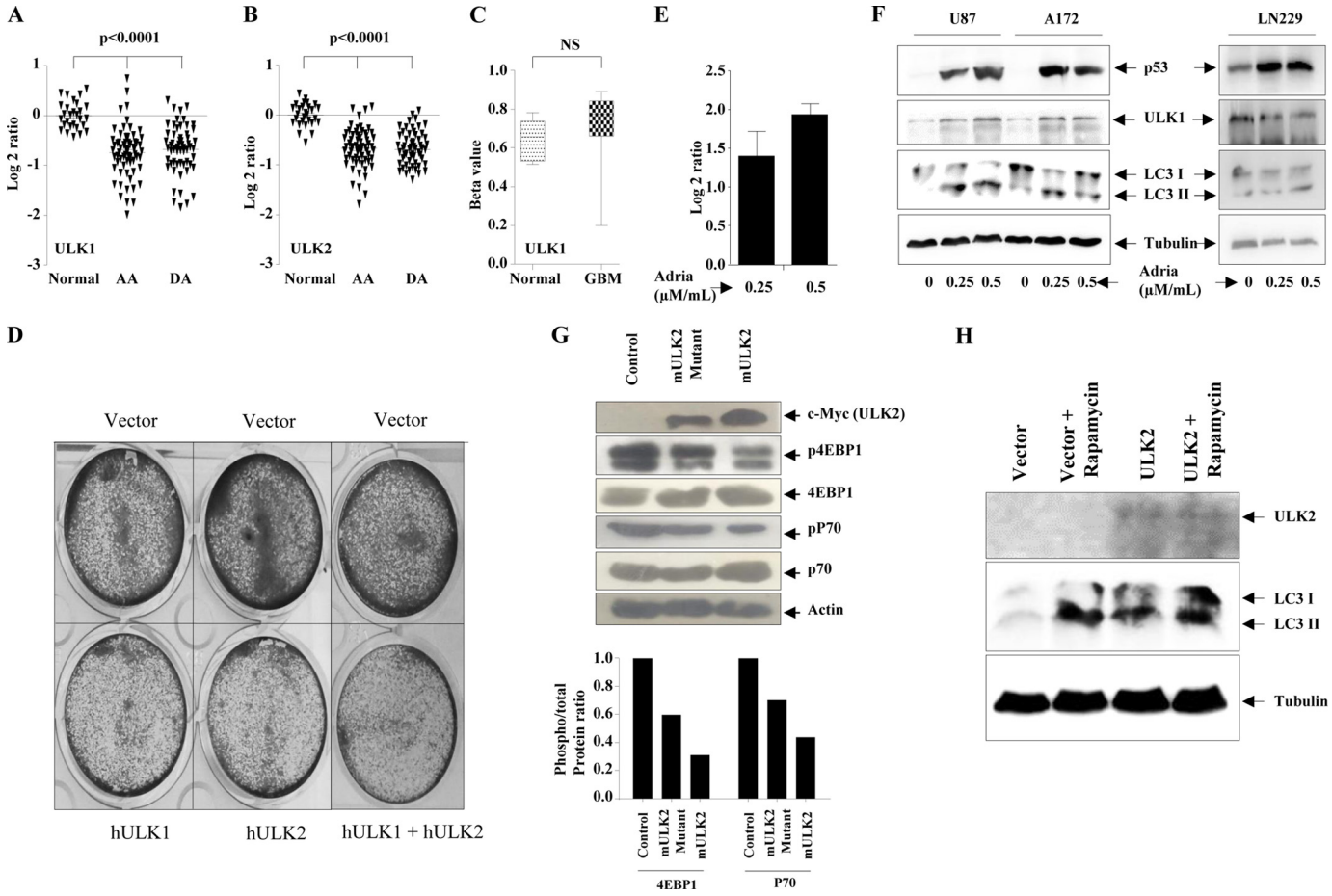

FIGURE 6. **ULK2 homolog ULK1, target of p53is also down-regulated and inhibits cell growth.** *A*, transcript level of ULK1 in different lower grades of glioma ($n = 227$) and normal brain samples ($n = 28$) obtained from the REMBRANDT dataset and plotted. The *t* test was performed between normal and different grades, and *p* values are indicated. *B*, transcript level of ULK2 in different lower grades of glioma ($n = 227$) and normal brain samples ($n = 28$) obtained from the REMBRANDT dataset and plotted. The *t* test was performed between normal and different grades, and *p* values are indicated. *C*, methylation levels (beta value) of ULK1 from normal brain samples ($n = 8$) and GBM ($n = 44$) were taken and plotted in a box plot. The *t* test was performed between normal brain samples and GBM, and *p* values are indicated (*NS* is not significant). *D*, LN229 cells were transfected with vector or hULK1 or hULK2 or equal amounts of hULK1 and hULK2 plasmids, and G418-resistant colonies were selected. Colonies were stained with crystal violet and photographed. *E*, total RNA was isolated from U87cell line after treatment with given concentrations of adriamycin, and the ULK1 transcript level was quantified by RT-qPCR. For each sample, the fold change in gene expression was calculated over its mean expression in untreated samples. *F*, total RNA was isolated from the U87 cell line after treatment with a given concentration (0.25 μg/ml and 0.5 μg/ml) of adriamycin and ULK1, p53, LC3 I/II, and tubulin protein levels were measured. *G*, total protein extracts of LN229/Vector or mutant mULK2 or mULK2 were isolated, and protein levels of indicated proteins were checked by Western blot. The ratio of phospho protein to total protein is shown in the *bar graph*. *H*, total protein extracts of LN229/Vector or mULK2 treated or untreated with rapamycin (10 μM), and levels of indicated proteins were checked by Western blot.

lation in glioma development needs further investigation (9, 20, 34, 35). In this study, we have compared methylation of GBM as a single group and also as G-CIMP+ and G-CIMP- groups separately with normal brain samples and identified both common and group-specific differentially methylated genes. In addition to finding the differential methylome common to all GBM, we also found G-CIMP+ and G-CIMP- GBM specific differential methylated genes. G-CIMP+ subset GBM are enriched for proneural expression types with good prognosis, while G-CIMP- subsets are enriched for classical and mesenchymal expression types with poor prognosis (6). In a good correlation gene ontology analysis, using group-specific differential methylome, we identified specific biological processes that are associated with these two subtypes are quite distinct and able to provide a biological explanation why these two classes of tumors are quite different in their aggressiveness and prognosis.

Of the differentially methylated genes in GBM, there were only three genes (RPL39L, ULK2, and HIST1H1A) that were hypermethylated and down-regulated in both groups of GBM. These three genes appear to be important in glioma development through their epigenetic regulation as they are methylation-silenced in GBM, while RPL39L has been found to be hypermethylated in prostate cancer (36). HIST1H1A, a member of linker histone H1, has been implicated in cisplatin resistance (37). ULK2 is one of the two mammalian homologues of UNC-51 of *Caenorhabditis elegans* and APG/Atg1 of *Saccharomyces cerevisiae* and is the upstream initiator of autophagy (38). The promoter methylation, and the consequent down-regulation of ULK2 expression was confirmed by multiple methods in this study. First, the infinium methylation array confirmed the ULK2 promoter methylation in three different datasets. Promoter methylation was further confirmed by bisulfite sequencing in both GBM tissue samples and glioma-derived cell lines. The transcript levels of ULK2 was also found to be down-regulated in three different datasets, and all glioma cell lines tested compared with normal brain

control samples. Additional confirmation came from the fact that glioma cell lines reexpressed ULK2 transcript upon methylation inhibitor treatment, and there was a significant negative correlation between ULK2 promoter methylation and transcript levels.

Autophagy is a lysosome-dependent bulk degradation of cytoplasmic components, in particular during starvation, for efficient utilization of cellular contents and has been shown to affect wide variety of diseases including cancer. However, there has been contradicting reports that autophagy has been shown to both promote cell survival and cell death (39, 40). While some studies support an oncogenic role, others appear to demonstrate a tumor suppressor role for autophagy. However, there is overwhelming evidence in the literature to suggest that autophagy is tumor-suppressive. There are several studies that support the observation that many molecules involved in induction, nucleation, elongation, and maturation step of autophagy have a tumor-suppressive role. While there are reports that suggest a dual function for autophagy in chemosensitivity of glioma cells (16–19), role of autophagy during glioma development has not been investigated. This study for the first time demonstrates that down-regulation of autophagy-initiating genes ULK1 and ULK2 is essential for autophagy inhibition during glioma development. We further show that down-regulation of ULK2 involves promoter methylation and consequent repression. We also demonstrate that p53 can activate ULK1 and hence p53 pathway inactivation, which happens in the majority of GBM (41) could be the reason behind ULK1 down-regulation in GBM.

Autophagy involves induction, nucleation, elongation, and maturation (40). After the induction step, vesicle nucleation is an important step in autophagy and is carried out in the complex consisting of PI3KC3, p150, Beclin1, UVRAG, Bif1, Ambra1, and ATG4 (40). Ectopic expression of Beclin1, a yeast homologue of Atg6/Vps30, has been shown to induce autophagy and suppress breast cancer cell growth (42). Monoallelic deficiency of Beclin1 is associated with tumor imitation and maintenance (42). Beclin1 heterozygous mice showed impaired autophagy and an increased propensity for developing spontaneous cancers (14, 42). Ectopic expression of UVRAG, the activator of Beclin1, has been shown to induce autophagy and suppress proliferation and tumorogenicity in colon cancer cell lines and found to be mutated in colorectal and gastric cancers (43–45). Mice lacking both alleles of Bif1, a UVRAG-interacting protein, enhanced the development of spontaneous tumors (46). We found that all these three genes: Beclin1, UVRAG. and Bif1 are neither down-regulated consistently nor deleted in glioblastoma (supplemental Figs. SF2 and SF3) thereby ruling out any role for these three genes in autophagy inhibition during astrocyte transformation.

The elongation step of autophagy involves two ubiquitin-like conjugation systems including Atg12, Atg8/LC3, Atg4C (also known as autophagin 3, a cysteine protease that cleaves Atg8), Atg7 (an E1 enzyme), Atg3 and Atg10 (E2 enzymes), and Atg16 (13). Mice lacking Atg4c show impaired autophagy and increased susceptibility to carcinogen-induced fibrosarcoma (3). Further, frameshift mutations in Atg5 were found to be common among microsatellite-instable (MSI-H) tumors and silencing of atg5 lead to genomic instability (47, 48). While the above data illustrates the important role played by the inactivation of these genes in cancer development, we found that Atg4c, Atg5, and many other genes of elongation step are neither down-regulated for their expression or deleted in glioblastoma (supplemental Fig. SF2 and SF3) thereby ruling out their role in autophagy inhibition during astrocyte transformation. In fact, we found the Atg3 and Atg4c to be up-regulated in glioblastoma compared with normal brain samples.

The Atg1 kinase complex plays a major role in the initiation of autophagy (induction step). In mammalian cells, this complex consists of ULK1, ULK2, Fused, Atg13, FIP200, and Atg101 (40). This complex is controlled by the nutrient sensor-mTOR, which phosphorylates ULK1/2 and Atg13 and inhibits autophagy. Since this complex appears to play an important role in controlling autophagy, genetic alterations in the members of this pathway would be expected in cancers as it would promote transformation. However, there have been no reports of genetic alterations in any of these genes in cancer as yet. While our study found that most genes in this complex are neither down-regulated nor deleted in glioblastoma, the transcript levels of ULK1, ULK2, and FIP200 are down-regulated significantly in glioblastoma compared with normal brain samples (supplemental Fig. SF2 and SF3), which suggest the down-regulation of these proteins may be important for autophagy inhibition to facilitate transformation during glioma development. However, mTOR(the inhibitor of Atg1 complex), which is constitutively activated by the PI3 kinase-Akt cascade in many cancers because of multiple upstream signaling from various tyrosine kinases as well as inactivation of inhibitors of this pathway, which include PTEN, AMPK, and TSC1/TSC2, can effectively inhibit autophagy (49). This would mean inactivation of Atg1 complex members may be redundant and may not be essential for autophagy inhibition during transformation.

However, Atg1 overexpression has been shown to inhibit mTOR activity using negative feedback loop leading to induction of autophagy and cell growth inhibition in *Drosophila* (24). The existence of a negative feedback loop between ULK1/2 and mTOR is further confirmed by the presence of activated mTOR in ULK1/2 double knock-out mice (50). Further, it has been shown that ULK1 and ULK2 inhibit mTORC1 by binding to and phosphorylating the raptor, the regulatory-associated protein of mTOR (51). In a good correlation, our results also indicate that overexpression of wild-type mULK2 inhibited mTOR activity as seen with reduced p4EBP1 and pP70 compared with the vector or kinase mutant form of mULK2 (Fig. 6*G*). Also, inhibition of mTOR signaling by rapamycin treatment increased ULK2-mediated autophagy (Fig. 6*H*), suggesting a role of mTOR in ULK2-mediated autophagy. The down-regulation of FIP200, another member of Atg1 complex, in glioblastoma may appear to downplay the importance of ULK1 and ULK2 down-regulation in autophagy inhibition to promote glioma development. However, the role of FIP200-induced autophagy has been shown to promote mammary tumorigenesis and support the maintenance of neural stem cells (52, 53). Hence, we believe that ULK1 and ULK2 down-regulation is more important as it not only leads to autophagy inhibition as well as acti-

vation of the mTOR complex, which is known for its positive role in transformation.

Thus, our study demonstrates for the first time that down-regulation of ULK1 and ULK2, the upstream autophagy activators, is essential for autophagy inhibition thus promoting transformation. While ULK2 down-regulation in GBM involves its promoter methylation, inactivated p53 pathway in GBM appears to be responsible for ULK1 down-regulation. Further, our study reinforces that autophagy is tumor-suppressive, and its inhibition is essential for astrocyte transformation.

Acknowledgments—The results published here are in whole or part based upon data generated by The Cancer Genome Atlas pilot project established by the NCI and NHGRI. The use of datasets from Institute NC, 2005 and Phillips et al., 2006 is acknowledged. Infrastructural support by funding from Indian Council of Medical Research, Department of Biotechnology, Department of Science, and University Grants Commission to the Department of Microbiology and Cell Biology is acknowledged. The Central Animal Facility of the Indian Institute of Science is acknowledged for animal experiments. We thank Professors M.R.S. Rao and P. Kondaiah for valuable suggestions. We thank Dr. H. Noushmehr for help in acquiring TCGA data. We also thank B. Thota, Shruti Bhargava, K. Chandrashekar, K. Prem, and B.C. Shailaja for the help rendered.

REFERENCES

1. Louis, D. N., Ohgaki, H., Wiestler, O. D., Cavenee, W. K., Burger, P. C., Jouvet, A., Scheithauer, B. W., and Kleihues, P. (2007) The 2007 WHO classification of tumours of the central nervous system. *Acta Neuropathol.* **114,** 97–109
2. Stupp, R., Hegi, M. E., Mason, W. P., van den Bent, M. J., Taphoorn, M. J., Janzer, R. C., Ludwin, S. K., Allgeier, A., Fisher, B., Belanger, K., Hau, P., Brandes, A. A., Gijtenbeek, J., Marosi, C., Vecht, C. J., Mokhtari, K., Wesseling, P., Villa, S., Eisenhauer, E., Gorlia, T., Weller, M., Lacombe, D., Cairncross, J. G., and Mirimanoff, R. O. (2009) Effects of radiotherapy with concomitant and adjuvant temozolomide versus radiotherapy alone on survival in glioblastoma in a randomised phase III study: 5-year analysis of the EORTC-NCIC trial. *Lancet Oncol.* **10,** 459–466
3. Nagarajan, R. P., and Costello, J. F. (2009) Epigenetic mechanisms in glioblastoma multiforme. *Semin Cancer Biol.* **19,** 188–197
4. Reddy, S. P., Britto, R., Vinnakota, K., Aparna, H., Sreepathi, H. K., Thota, B., Kumari, A., Shilpa, B. M., Vrinda, M., Umesh, S., Samuel, C., Shetty, M., Tandon, A., Pandey, P., Hegde, S., Hegde, A. S., Balasubramaniam, A., Chandramouli, B. A., Santosh, V., Kondaiah, P., Somasundaram, K., and Rao, M. R. (2008) Novel glioblastoma markers with diagnostic and prognostic value identified through transcriptome analysis. *Clinical Cancer Research* **14,** 2978–2987
5. Sreekanthreddy, P., Srinivasan, H., Kumar, D. M., Nijaguna, M. B., Sridevi, S., Vrinda, M., Arivazhagan, A., Balasubramaniam, A., Hegde, A. S., Chandramouli, B. A., Santosh, V., Rao, M. R., Kondaiah, P., and Somasundaram, K. (2010) Identification of potential serum biomarkers of glioblastoma: serum osteopontin levels correlate with poor prognosis. *Cancer Epidemiol. Biomarkers Prev.* **19,** 1409–1422
6. Noushmehr, H., Weisenberger, D. J., Diefes, K., Phillips, H. S., Pujara, K., Berman, B. P., Pan, F., Pelloski, C. E., Sulman, E. P., Bhat, K. P., Verhaak, R. G., Hoadley, K. A., Hayes, D. N., Perou, C. M., Schmidt, H. K., Ding, L., Wilson, R. K., Van Den Berg, D., Shen, H., Bengtsson, H., Neuvial, P., Cope, L. M., Buckley, J., Herman, J. G., Baylin, S. B., Laird, P. W., and Aldape, K. (2010) Identification of a CpG island methylator phenotype that defines a distinct subgroup of glioma. *Cancer Cell* **17,** 510–522
7. Bird, A. P. (1986) CpG-rich islands and the function of DNA methylation. *Nature* **321,** 209–213
8. Gonzalez-Gomez, P., Bello, M. J., Arjona, D., Lomas, J., Alonso, M. E., De Campos, J. M., Vaquero, J., Isla, A., Gutierrez, M., and Rey, J. A. (2003) Promoter hypermethylation of multiple genes in astrocytic gliomas. *Int. J. Oncol.* **22,** 601–608
9. Foltz, G., Ryu, G. Y., Yoon, J. G., Nelson, T., Fahey, J., Frakes, A., Lee, H., Field, L., Zander, K., Sibenaller, Z., Ryken, T. C., Vibhakar, R., Hood, L., and Madan, A. (2006) Genome-wide analysis of epigenetic silencing identifies BEX1 and BEX2 as candidate tumor suppressor genes in malignant glioma. *Cancer Res.* **66,** 6665–6674
10. Garcia-Manero, G. (2008) Demethylating agents in myeloid malignancies. *Curr. Opin. Oncol.* **20,** 705–710
11. Kroemer, G., Mariño, G., and Levine, B. (2010) Autophagy and the integrated stress response. *Mol. Cell* **40,** 280–293
12. Codogno, P., and Meijer, A. J. (2005) Autophagy and signaling: their role in cell survival and cell death. *Cell Death Differ.* **12,** 1509–1518
13. Degenhardt, K., Mathew, R., Beaudoin, B., Bray, K., Anderson, D., Chen, G., Mukherjee, C., Shi, Y., Gélinas, C., Fan, Y., Nelson, D. A., Jin, S., and White, E. (2006) Autophagy promotes tumor cell survival and restricts necrosis, inflammation, and tumorigenesis. *Cancer Cell* **10,** 51–64
14. Qu, X., Yu, J., Bhagat, G., Furuya, N., Hibshoosh, H., Troxel, A., Rosen, J., Eskelinen, E. L., Mizushima, N., Ohsumi, Y., Cattoretti, G., and Levine, B. (2003) Promotion of tumorigenesis by heterozygous disruption of the beclin 1 autophagy gene. *J. Clin. Invest.* **112,** 1809–1820
15. Kaza, N., Kohli, L., and Roth, K. A. (2012) Autophagy in brain tumors: a new target for therapeutic intervention. *Brain Pathol.* **22,** 89–98
16. Kanzawa, T., Germano, I. M., Komata, T., Ito, H., Kondo, Y., and Kondo, S. (2004) Role of autophagy in temozolomide-induced cytotoxicity for malignant glioma cells. *Cell Death Differ.* **11,** 448–457
17. Arcella, A., Biagioni, F., Antonietta Oliva, M., Bucci, D., Frati, A., Esposito, V., Cantore, G., Giangaspero, F., and Fornai, F. (2013) Rapamycin inhibits the growth of glioblastoma. *Brain Res.* **1495,** 37–51
18. McAfee, Q., Zhang, Z., Samanta, A., Levi, S. M., Ma, X. H., Piao, S., Lynch, J. P., Uehara, T., Sepulveda, A. R., Davis, L. E., Winkler, J. D., and Amaravadi, R. K. (2012) Autophagy inhibitor Lys05 has single-agent antitumor activity and reproduces the phenotype of a genetic autophagy deficiency. *Proc. Natl. Acad. Sci. U.S.A.* **109,** 8253–8258
19. Hu, Y. L., DeLay, M., Jahangiri, A., Molinaro, A. M., Rose, S. D., Carbonell, W. S., and Aghi, M. K. (2012) Hypoxia-induced autophagy promotes tumor cell survival and adaptation to antiangiogenic treatment in glioblastoma. *Cancer Res.* **72,** 1773–1783
20. Shukla, S., Pia Patric, I. R., Thinagararjan, S., Srinivasan, S., Mondal, B., Hegde, A. S., Chandramouli, B. A., Santosh, V., Arivazhagan, A., and Somasundaram, K. (2013) A DNA methylation prognostic signature of glioblastoma: identification of NPTX2-PTEN-NF-kappaB nexus. *Cancer Res.* **73,** 6563–6573
21. Issa, J. P. (2004) CpG island methylator phenotype in cancer. *Nature Reviews. Cancer* **4,** 988–993
22. Baehrecke, E. H. (2005) Autophagy: dual roles in life and death? *Nature Reviews. Mol. Cell Biol.* **6,** 505–510
23. Guo, J. Y., Chen, H. Y., Mathew, R., Fan, J., Strohecker, A. M., Karsli-Uzunbas, G., Kamphorst, J. J., Chen, G., Lemons, J. M., Karantza, V., Coller, H. A., Dipaola, R. S., Gelinas, C., Rabinowitz, J. D., and White, E. (2011) Activated Ras requires autophagy to maintain oxidative metabolism and tumorigenesis. *Genes Dev.* **25,** 460–470
24. Scott, R. C., Juhász, G., and Neufeld, T. P. (2007) Direct induction of autophagy by Atg1 inhibits cell growth and induces apoptotic cell death. *Curr. Biol.* **17,** 1–11
25. Yu, L., Wan, F., Dutta, S., Welsh, S., Liu, Z., Freundt, E., Baehrecke, E. H., and Lenardo, M. (2006) Autophagic programmed cell death by selective catalase degradation. *Proc. Natl. Acad. Sci. U.S.A.* **103,** 4952–4957
26. Wang, R. C., Wei, Y., An, Z., Zou, Z., Xiao, G., Bhagat, G., White, M., Reichelt, J., and Levine, B. (2012) Akt-mediated regulation of autophagy and tumorigenesis through Beclin 1 phosphorylation. *Science* **338,** 956–959
27. Cho, D. H., Jo, Y. K., Kim, S. C., Park, I. J., and Kim, J. C. (2012) Down-regulated expression of ATG5 in colorectal cancer. *Anticancer Res.* **32,** 4091–4096
28. Gao, W., Shen, Z., Shang, L., and Wang, X. (2011) Upregulation of human autophagy-initiation kinase ULK1 by tumor suppressor p53 contributes to

DNA-damage-induced cell death. *Cell Death Differ.* **18,** 1598–1607
29. Ehrlich, M. (2002) DNA methylation in cancer: too much, but also too little. *Oncogene* **21,** 5400–5413
30. Ehrlich, M. (2002) DNA hypomethylation, cancer, the immunodeficiency, centromeric region instability, facial anomalies syndrome and chromosomal rearrangements. *J. Nutrition* **132,** 2424S-2429S
31. Fu, T., Pappou, E. P., Guzzetta, A. A., Jeschke, J., Kwak, R., Dave, P., Hooker, C. M., Morgan, R., Baylin, S. B., Iacobuzio-Donahue, C. A., Wolfgang, C. L., and Ahuja, N. (2012) CpG island methylator phenotype-positive tumors in the absence of MLH1 methylation constitute a distinct subset of duodenal adenocarcinomas and are associated with poor prognosis. *Clinical Cancer Research* **18,** 4743–4752
32. Toyota, M., Ahuja, N., Ohe-Toyota, M., Herman, J. G., Baylin, S. B., and Issa, J. P. (1999) CpG island methylator phenotype in colorectal cancer. *Proc. Natl. Acad. Sci. U.S.A.* **96,** 8681–8686
33. Turcan, S., Rohle, D., Goenka, A., Walsh, L. A., Fang, F., Yilmaz, E., Campos, C., Fabius, A. W., Lu, C., Ward, P. S., Thompson, C. B., Kaufman, A., Guryanova, O., Levine, R., Heguy, A., Viale, A., Morris, L. G., Huse, J. T., Mellinghoff, I. K., and Chan, T. A. (2012) IDH1 mutation is sufficient to establish the glioma hypermethylator phenotype. *Nature* **483,** 479–483
34. Kim, S. J., Choi, H. J., Jin, U. H., Lee, Y. C., and Kim, C. H. (2006) Transcriptional regulation of the human Sia-α2,3-Gal-β1,4-GlcNAc-R:α2,8-sialyltransferase (hST8Sia III) by retinoic acid in human glioblastoma tumor cell line. *Biochim. Biophys. Acta* **1759,** 451–457
35. Martinez, R., Martin-Subero, J. I., Rohde, V., Kirsch, M., Alaminos, M., Fernandez, A. F., Ropero, S., Schackert, G., and Esteller, M. (2009) A microarray-based DNA methylation study of glioblastoma multiforme. *Epigenetics* **4,** 255–264
36. Devaney, J. M., Wang, S., Funda, S., Long, J., Taghipour, D. J., Tbaishat, R., Furbert-Harris, P., Ittmann, M., and Kwabi-Addo, B. (2013) Identification of novel DNA-methylated genes that correlate with human prostate cancer and high-grade prostatic intraepithelial neoplasia. *Prostate Cancer Prostatic Diseases* **16,** 292–300
37. Wu, Z. Z., Lu, H. P., and Chao, C. C. (2010) Identification and functional analysis of genes which confer resistance to cisplatin in tumor cells. *Biochem. Pharmacol.* **80,** 262–276
38. Lee, E. J., and Tournier, C. (2011) The requirement of uncoordinated 51-like kinase 1 (ULK1) and ULK2 in the regulation of autophagy. *Autophagy* **7,** 689–695
39. Rosenfeldt, M. T., and Ryan, K. M. (2011) The multiple roles of autophagy in cancer. *Carcinogenesis* **32,** 955–963
40. Liang, C., and Jung, J. U. (2010) Autophagy genes as tumor suppressors. *Curr. Opin. Cell Biol.* **22,** 226–233
41. Cancer Genome Atlas Research, N. (2008) Comprehensive genomic characterization defines human glioblastoma genes and core pathways. *Nature* **455,** 1061–1068
42. Liang, X. H., Jackson, S., Seaman, M., Brown, K., Kempkes, B., Hibshoosh, H., and Levine, B. (1999) Induction of autophagy and inhibition of tumorigenesis by beclin 1. *Nature* **402,** 672–676
43. Liang, C., Feng, P., Ku, B., Dotan, I., Canaani, D., Oh, B. H., and Jung, J. U. (2006) Autophagic and tumour suppressor activity of a novel Beclin1-binding protein UVRAG. *Nature Cell Biology* **8,** 688–699
44. Goi, T., Kawasaki, M., Yamazaki, T., Koneri, K., Katayama, K., Hirose, K., and Yamaguchi, A. (2003) Ascending colon cancer with hepatic metastasis and cholecystolithiasis in a patient with situs inversus totalis without any expression of UVRAG mRNA: report of a case. *Surgery Today* **33,** 702–706
45. Kim, M. S., Jeong, E. G., Ahn, C. H., Kim, S. S., Lee, S. H., and Yoo, N. J. (2008) Frameshift mutation of UVRAG, an autophagy-related gene, in gastric carcinomas with microsatellite instability. *Human Pathology* **39,** 1059–1063
46. Takahashi, Y., Coppola, D., Matsushita, N., Cualing, H. D., Sun, M., Sato, Y., Liang, C., Jung, J. U., Cheng, J. Q., Mulé, J. J., Pledger, W. J., and Wang, H. G. (2007) Bif-1 interacts with Beclin 1 through UVRAG and regulates autophagy and tumorigenesis. *Nature Cell Biology* **9,** 1142–1151
47. Karantza-Wadsworth, V., Patel, S., Kravchuk, O., Chen, G., Mathew, R., Jin, S., and White, E. (2007) Autophagy mitigates metabolic stress and genome damage in mammary tumorigenesis. *Genes Dev.* **21,** 1621–1635
48. Kang, M. R., Kim, M. S., Oh, J. E., Kim, Y. R., Song, S. Y., Kim, S. S., Ahn, C. H., Yoo, N. J., and Lee, S. H. (2009) Frameshift mutations of autophagy-related genes ATG2B, ATG5, ATG9B and ATG12 in gastric and colorectal cancers with microsatellite instability. *J. Pathol.* **217,** 702–706
49. Shaw, R. J., and Cantley, L. C. (2006) Ras, PI(3)K and mTOR signalling controls tumour cell growth. *Nature* **441,** 424–430
50. Cheong, H., Wu, J., Gonzales, L. K., Guttentag, S. H., Thompson, C. B., and Lindsten, T. (2014) Analysis of a lung defect in autophagy-deficient mouse strains. *Autophagy* **10,** 45–56
51. Jung, C. H., Seo, M., Otto, N. M., and Kim, D. H. (2011) ULK1 inhibits the kinase activity of mTORC1 and cell proliferation. *Autophagy* **7,** 1212–1221
52. Wang, C., Liang, C. C., Bian, Z. C., Zhu, Y., and Guan, J. L. (2013) FIP200 is required for maintenance and differentiation of postnatal neural stem cells. *Nature Neuroscience* **16,** 532–542
53. Wei, H., Wei, S., Gan, B., Peng, X., Zou, W., and Guan, J. L. (2011) Suppression of autophagy by FIP200 deletion inhibits mammary tumorigenesis. *Genes Dev.* **25,** 1510–1527